AIMS Geosciences

AIMS Geosciences, 12(1): 127–157.
DOI: 10.3934/geosci.2026005
Received: 09 July 2025
Revised: 14 November 2025
Accepted: 27 December 2025
Published: 26 January 2026

https://www.aimspress.com/journal/geosciences

Research article

A GIS-enabled AHP approach for mapping urban flood susceptibility in Bhubaneswar city

Monashree Panigrahi, Sudhakar Pal and Arabinda Sharma*

School of Geography, Gangadhar Meher University, Sambalpur-768004, Odisha, India

* **Correspondence**: Email: asharma@gmuniversity.ac.in; Tel:7077098547.

Abstract: Urban floods are among the most devastating natural disasters, causing severe damage to human life, property, and the economy. In this study, we focused on mapping Urban Flood Susceptibility Zones (UFSZ) within the Bhubaneswar Municipal Corporation (BMC), as it used a GIS-based Analytical Hierarchy Process (AHP) model integrated via Remote Sensing (RS) with Multi-Criteria Decision-Making (MCDM) techniques. Twelve flood-inducing factors were given weight by the model. Elevation had 25%, Land Use and Land Cover had 19%, and Distance to River received 15%, marking these as critical parameters. We analyzed 130 flood event locations collected through field surveys conducted between June and September 2023, validating flood-prone zones using the Google Earth Engine (GEE). A Consistency Ratio (CR) of 0.06 (<0.1) confirmed the reliability of the weight calculations. The results showed that 45.82% of the area of Bhubaneswar lies within the southern, southeastern, and central parts of the city that are identified under high to very high flood susceptibility zones. This research uniquely fulfils the need for a high-resolution flood susceptibility map and provides crucial insight to city planners and policymakers for improving urban flood resilience, urban infrastructure development, and flood disaster risk management.

Keywords: AHP; urban flood; susceptibility mapping; bhubaneswar municipal region (BMR); GIS; remote sensing

Abbreviation: Elevation (E), Curvature (Cu), Aspect (As), Annual Rainfall (AR), Land use and Landcover (LULC), Soil type (So), Topographic Wetness Index (TWI), Distance to River (DTR),

Normalized Difference Vegetation Index (NDVI), Normalized Difference Built-up Index (NDBI), Normalized Difference Water Index (NDWI) and Topographic Position Index (TPI).

1. Introduction

The environmental dilemma resulting from excessive rainfall in metropolitan settings has become a significant global issue. Urban flooding is among the most frequent and destructive phenomena and is expected to occur with increased frequency in urban areas as a result of climate change and accelerated urbanization. Urban precipitation and ensuing urban waterlogging are a widespread disaster that elicits harmful physical and socio-economic obstacles in metropolitan environments [1]. More than 30% of the economic losses and victims from annual natural disasters are caused by floods [2]. Flooding is, therefore, among the most devastating hazards on earth, posing significant threats to a large portion of the world. Rainstorms or intense rainfall of short duration often trigger runoff that exceeds urban drainage systems' flow capacity, leading to urban waterlogging catastrophes [3]. This phenomenon is particularly prevalent during the monsoon season in metropolitan areas, especially in developing nations. Indian cities are more susceptible than any other developed nation because of rapid population growth outpacing urban infrastructure, leading to insufficient adaptation measures and a heightened risk of seasonal floods [4]. There has been a significant increase in urban waterlogging and flooding in Indian cities over the past few years, notably impacting cities such as Chennai [5], Mumbai [6], Kolkata [7], Siliguri, Navsari [8], Bhopal [9], Gurgaon, and Delhi. Bhubaneswar, the capital city of Odisha, is one such rapidly urbanizing tier-II Indian city where urban flooding has become a growing concern, primarily driven by unplanned development, insufficient drainage infrastructure, and heavy monsoonal rains.

Mapping and understanding of urban flood susceptibility at a refined scale is in great demand, more so in the case of medium-sized Indian urban centres, where the rate of urbanization is furiously high and town planning is virtually non-existent. Rapid assessment of floods is crucial for effective disaster management and climate-resilient approaches. In a major step forward, flood assessments are greatly enhanced through the coupled use of Geographic Information Systems (GIS) and Remote Sensing (RS) techniques. According to [10] and [11], RS and GIS platforms enhance the precision of flood mapping by integrating spatial and temporal datasets. Over the past decades, scholars have used different statistical methods along with RS and GIS to discover the most plausible, rational, and reliable results. Commonly used statistical techniques are the analytical hierarchy process (AHP) [12], weights-of-evidence, frequency ratio (FR), fuzzy logic, logistic regression, artificial neural network (ANN), decision tree, evidential belief function (EBF), adaptive neuro fuzzy inference system, and support vector machine (SVM) [13].

International studies [14] show that hybrid geospatial approaches analyze complex flood scenarios with particular effectiveness, while Indian studies [15] highlight that there is an increasing need to integrate geospatial data into multi-criteria decision-making (MCDM) techniques. Following this, the reseachers in [16] studied peri-urban north Bhubaneswar using a GRID analysis via GIS. Their work underscored just how land-use change, along with impervious surface expansion, strengthens flood vulnerability. At the global scale, the researchers in [17] provide a systematic review of urban flood susceptibility mapping approaches, comparing remote sensing, machine learning, and hybrid MCDM methods, and highlighting each method's relative strengths and limitations. Within India, [18] Ahmed Khan and Jhamnani (2023) applied GIS-AHP to the Idukki

district because it presents adaptability across physical terrains and reinforces methodological relevance for flood susceptibility studies.

Among MCDM techniques, AHP remains one of the widely used approaches for determining criteria weights because of its logical pairwise comparison process and theoretical foundation [19,20] and has been successfully used in multiple environmental and risk studies due to its ability to normalize the parameters, articulate uncertainties in the decision-making process, and offer clear weighting structures [21,22]. The integration of AHP with GIS in geographic flood studies enhances the utility of AHP, which organizes flood drivers in order of importance, and GIS focuses on the spatial integration of drivers, visualization, and analysis. This coupled functionality makes the AHP–GIS framework for urban flood studies instrumental, given the decision-centric nature of the problem and the need for high spatial accuracy.

Based on the above context, w,e adopted geographical mapping of urban flood susceptibility using an AHP-GIS framework to map Bhubaneswar, an Indian city prone to flooding and rapid urbanization, as a key case study. Although more studies have been made on flood susceptibility in India, there remains a critical knowledge gap because they tend to either assess the region at a broader scale or use older datasets, thus ignoring the localized flood patterns and dynamics of urban morphology in tier-II towns. Moreover, several researchers tend to focus more on the integration of socio-economic drivers and lack emphasis on the physical environment alone, which is a very essential pre-step for drainage upgrades and infrastructure planning.

Thus, our research objectives are to develop a fine-scale AHP-GIS framework to assess flood susceptibility in Bhubaneswar. The novelty of this work lies in (i) our focus on a rapidly urbanizing tier-II city in India, (ii) the application of twelve updated physical-geospatial indicators, and (iii) validation of outcomes through 130 flood field observations and GEE-SAR-based flood mapping. Focusing on the physical-environmental drivers provides infrastructure-relevant outcomes but can easily incorporate the socio-economic factors in the future. The resulting susceptibility map is expected to enhance ward-level disaster preparedness, zoning regulations, and drainage system planning in Bhubaneswar and serve as a transferable model for other medium-sized cities in South Asia.

2. Materials and methods

In this section, we present the data used and the methodological frameworks employed to create a flood susceptibility map for the study region.

2.1. Study area

Bhubaneswar city (20° 17’ 45” N, 85° 49’ 28” E), the capital of Odisha (Figure 1c), covers 145.55 km^2 and is the most important economic and administrative hub in the country.

The city is situated between the Chandaka reserve forest to the west, the Kuakhai river to the east, and the Daya river to the southeast. It has four micro water basins with a dominant slope extending from west to east, and ten natural streams that have been transformed into nallas for transporting sewage and stormwater. Gangua Nalla in the east serves as the primary conduit for discharging wastewater, rainwater, industrial effluents, and contaminants into the Daya River.

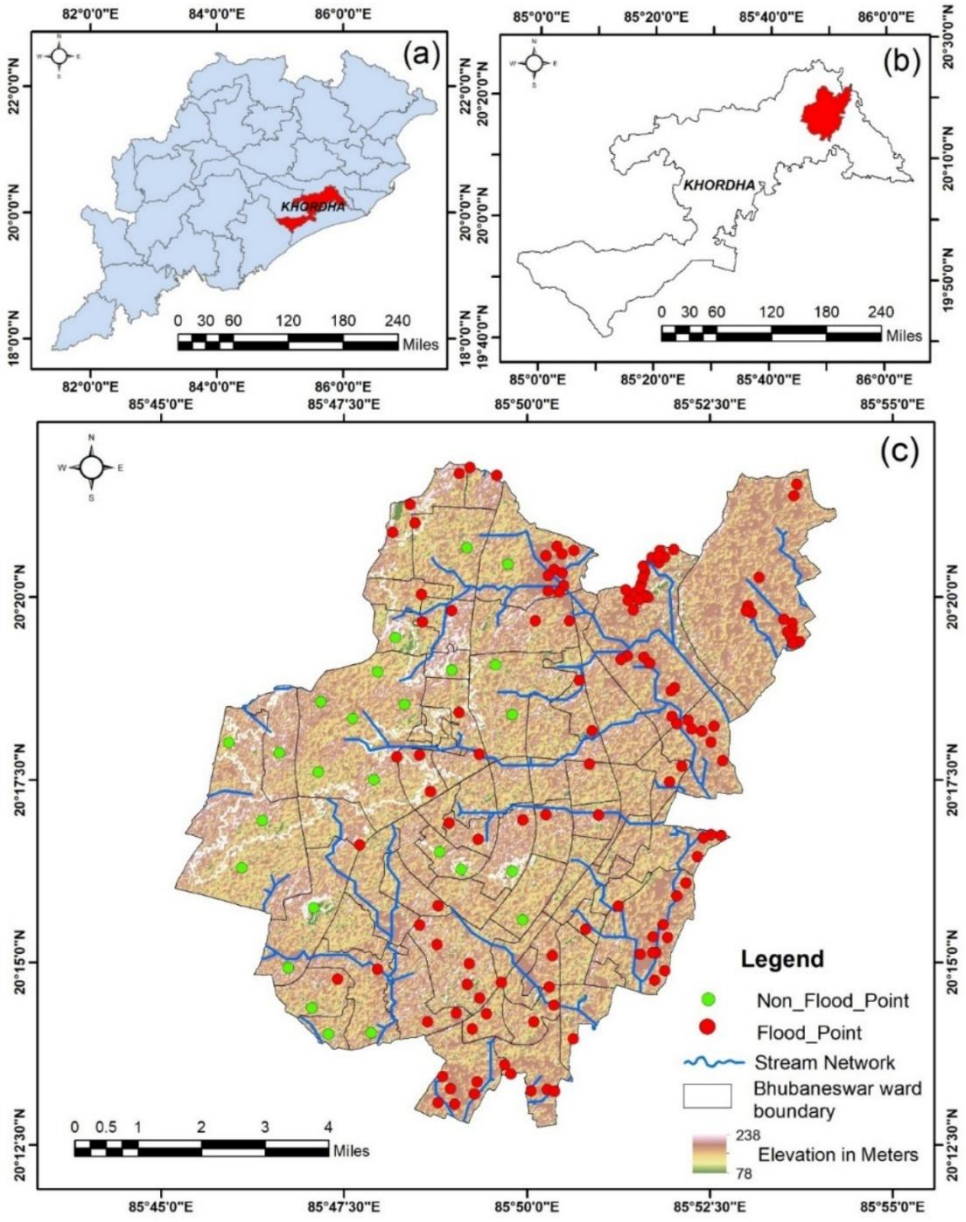

Figure 1. Location of the study area in the eastern Indian state of Odisha, along with elevation, drainage, and historical flood points.

The city experiences an average annual precipitation of 1,497 mm, with a rainy season from May to October. By 2010, the average number of rainy days was 87, which decreased to 75 by 2011. According to the report, Bhubaneswar (Hazard Risk and Vulnerability Analysis (HRVA), 2014) of the city of Bhubaneswar (Odisha), 2014, released by BMC, 2014, since 2010, Bhubaneswar has experienced localized flooding or waterlogging issues due to factors such as rapid infrastructure and population growth, encroachment, siltation, debris dumping, and conversion of flood plains into residential areas. These issues disrupt daily activities and create havoc in areas like Acharya Bihar, Jayadev Bihar, Chandrasekharpur, Rangamatia, and Salia Sahi. Frequent urban flood disasters have caused large economic losses and threatened the safety of people's lives and property. As Bhubaneswar

city aims to be a smart city, a detailed flood assessment study is necessary to address these challenges and ensure the safety of its residents and property.

2.2. Experimental data

After the selection of the study area and conducting a thorough literature review, twelve flash flood influencing factors, namely, E, Cu, As, AR, LULC, So, TWI, DTR, NDVI, NDBI, NDWI, and TPI, were considered for the flash flood susceptibility mapping [23–25]. The complete details of these data sources are mentioned in Table 1.

Although socio-economic indicators (e.g., population density, infrastructure, and household vulnerability) are widely used in integrated flood risk models, we deliberately excluded them to focus on the physical-environmental drivers of urban flooding. The rationale was to develop a framework directly applicable to drainage design, infrastructure upgrades, and physical hazard assessment. In future work, researcheres could integrate socio-economic indicators to generate coupled risk models.

Table 1. Data collection and preparation.

Sl No	Derived Parameters	Primary Source	Resolution	Equation	Reference
1	Elevation (E)	Alos Palsar DEM (https:// search. asf. alaska. edu/)	12.5 m × 12.5 m	Elevation $= z(x, y)$ Where: $z(x, y)$ is the elevation value stored in the DEM at the grid location corresponding to the coordinates? (x, y).	[26]
2	Aspect (As)	Alos Palsar DEM	12.5 m × 12.5 m	$\text{Aspect} = \arctan\left(\frac{-\frac{\partial Z}{\partial y}}{\frac{\partial Z}{\partial x}}\right)$ Where: $\frac{\partial Z}{\partial x}$: Rate of change of elevation in the east-west direction (slope in the x-direction). $\frac{\partial Z}{\partial y}$: Rate of change of elevation in the north-south direction (slope in the y-direction).	[26]
3	Curvature (Cu)	Alos Palsar DEM	12.5 m × 12.5 m	$C = \frac{z_{xx} \cdot z_y^2 - 2 \cdot z_x \cdot z_y \cdot z_{xy} + z_{yy} \cdot z_x^2}{z_x^2 + z_y^2}$ Where: • z_x and z_y are 1st-order slope components in the x and y directions. • z_{xx}, z_{yy}, z_{xy} are 2nd-order partial derivatives calculated from the elevation data.	[27]
4	Distance to River (DTR)	Bhukosh GSI Portal (https:// bhuko sh. gsi. gov. in/)	-	Extracted from vector drainage map	[28]

Continued on next page

Sl No	Derived Parameters	Primary Source	Resolution	Equation	Reference
5	Soil type	NBSS& LUP Portal (https://www.bhoomigeoportal-nbsslup.in/)	-	Categorical data from soil maps	[29]
6	NDVI	Sentinel-2A (https://www.sentinel-hub.com)	10 m × 10 m	$\mathrm{NDVI} = \frac{(\mathrm{NIR} - \mathrm{RED})}{(\mathrm{NIR} + \mathrm{RED})}$ Where: • NIR (Near-Infrared): Band 8 and RED (Red): Band 4 of Sentinel-2A	[30]
7	NDBI	Sentinel-2A	10 m × 10 m	$\mathrm{NDBI} = \frac{(\mathrm{SWIR} - \mathrm{NIR})}{(\mathrm{SWIR} + \mathrm{NIR})}$ Where: • SWIR (Short-Wave Infrared) corresponds to Band 11 and NIR (Near-Infrared): Band 8 of Sentinel-2	[31]
8	NDWI	Sentinel-2A	10 m × 10 m	$\mathrm{NDBI} = \frac{(\mathrm{Green} - \mathrm{NIR})}{(\mathrm{Green} + \mathrm{NIR})}$ Where: • Green (Band 3) and NIR (Band 8) in Sentinel-2A	[32]
9	LULC	Sentinel-2A	10 m × 10 m	$OA = (n\|N) * 100$ • n: Number of correctly classified points based on Sentinel-2A classification. • N: Total number of validation points (ground truth). $K = \frac{\mathrm{N}\sum_{i=1}^{r} X_{ii} - \sum_{i=1}^{r}(X_{i+}X + i)}{N^2 - \sum_{i=1}^{r}(X_{i+}X + i)}$ • N^2 denotes the square of total number of samples • X_{i+} refers to the column total • X_{+i} represents the row total • r signifies the number of rows in the error matrix	[30]
10	AR	IMD Gridded rainfall (https:// bhukosh. gsi. gov. in/)	(0.25° × 0.25°)	Annual rainfall (mm/year)	[33]
11	TWI	Alos Palsar DEM	12.5 m × 12.5 m	$\mathrm{TWI} = \mathrm{Ln}\left(\frac{a}{\tan B}\right)$ where a and B represent the specific catchment area and slope of the region, respectively.	[34]
12	TPI	Alos Palsar DEM	12.5 m × 12.5 m	$\mathrm{TPI} = Z_0 - \frac{1}{n}\sum_{i=1}^{n} Z_i$ Z_0: Elevation of the central cell (target cell) Z_i: Elevation of the surrounding cells (neighbouring cells) n: Total number of neighbouring cells	[35]

The temporal and spatial details of all datasets are summarized in Table 1. Datasets were chosen to align as closely as possible with the flood events recorded during June–September 2023, ensuring temporal consistency. Sentinel-2A imagery (06-07-2023), IMD gridded rainfall data (2022–2023), and ALOS-PALSAR DEM (2011 static) were used.

2.3. Methodology

We used a set of MCDM approaches within the AHP framework to forecast flood susceptibility based on geographical predictors and historical flood occurrences (both flood and non-flood sites) (Figure 1c). Furthermore, Figure 2 indicates the detailed methodology adopted in this research.

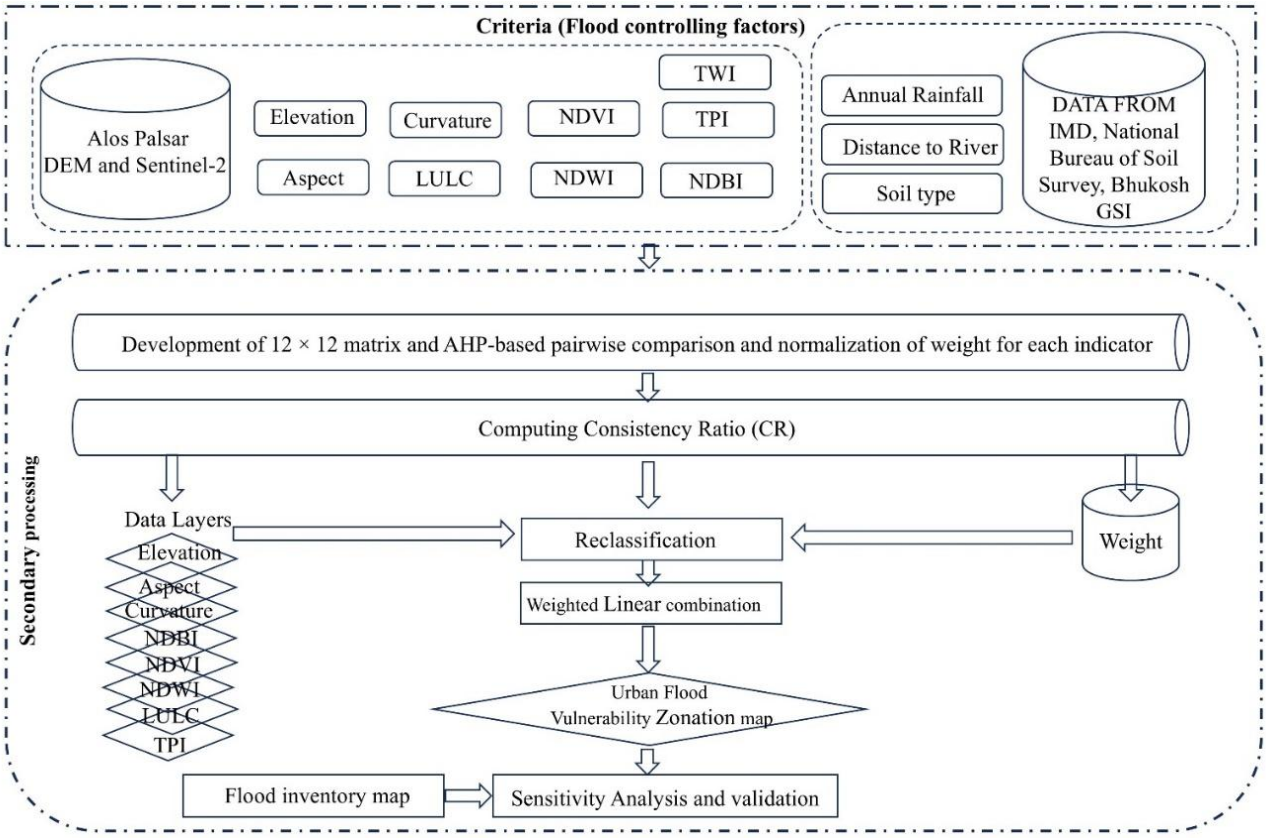

Figure 2. Flowchart of the methodology.

2.3.1. Flood inventory map

Generating a flood inventory map was considered an essential step in assessing the flood likelihood. A flood inventory map of BMC was created, featuring 130 flood event locations, which were obtained from a rigorous field study conducted during the monsoon period (June 2023–September 2023). Each point was recorded with GPS coordinates, severity level (low, medium, high), and supported by photographic evidence. To reduce reporting bias, locations were verified through structured interviews with residents and cross-checked against Google Earth Engine cloud datasets. The 130 points were classified into flash flood points and non-flash flood points, and this Flood Inventory Map (Figure 3) serves as the validation dataset for susceptibility modeling.

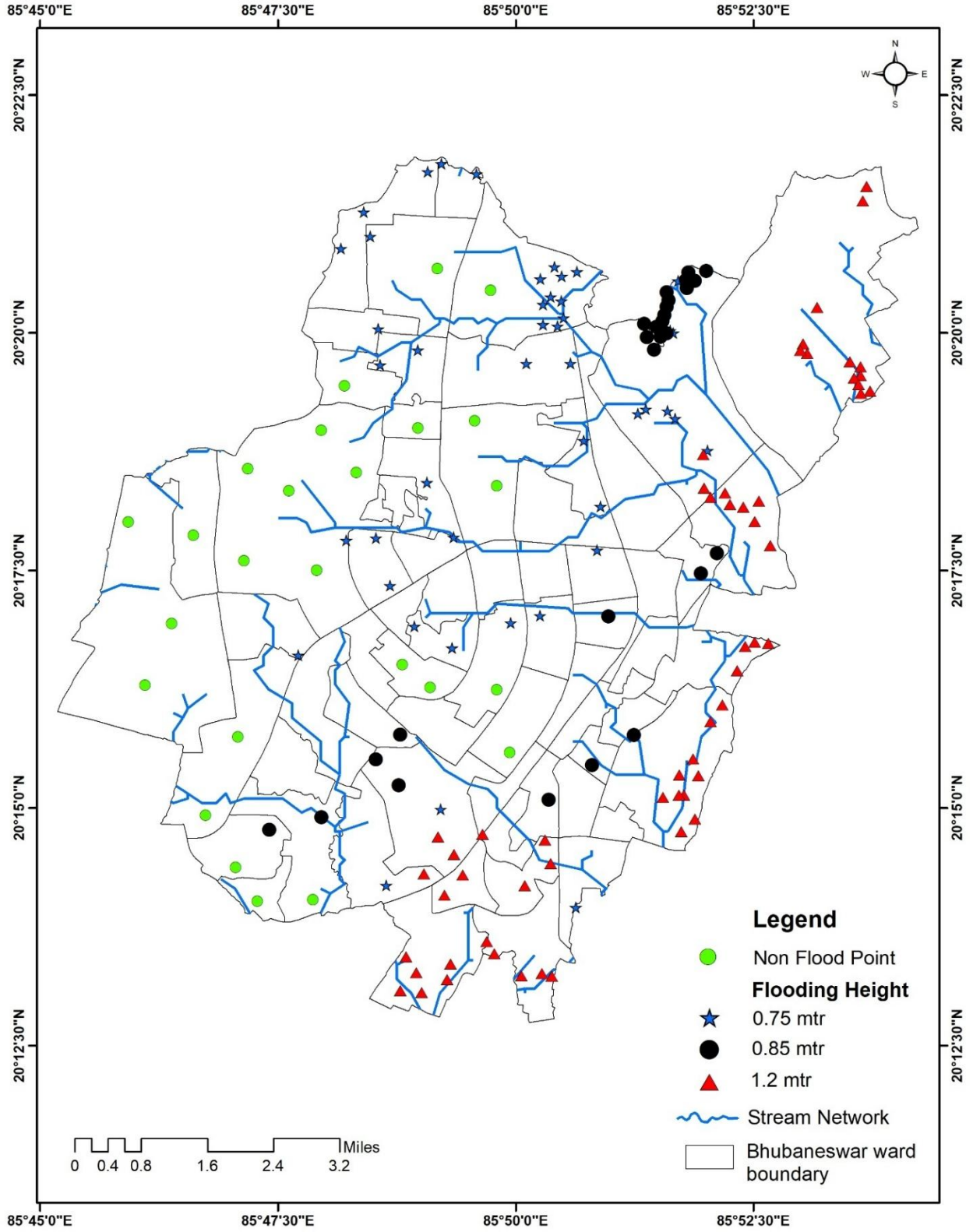

Figure 3. Flood inventory map.

2.3.2. Identification of influencing factors for urban flood susceptibility

2.3.2.1. Flood parameter selection

The selection of indicator elements was a crucial phase in the multi-index flood risk assessment procedure. The susceptibility risk assessment of urban flooding in the BMR was performed using multi-source spatial data [36]. Twelve factors influencing urban flood risk were identified for the study region based on the current literature [37] and guidance from the domain experts. The parameters are E, Cu, As, AR, LULC, So, TWI, DTR, NDVI, NDBI, NDWI, and TPI. The Alos Palsar digital elevation model (DEM) was used to create physical thematic layers for the study region (as shown in Table 1). Satellite imagery from Sentinel-2A was used after pre-processing, and NDVI, NDBI, and NDWI were derived from Sentinel-2A. River information, annual rainfall, and soil type were also gathered from publicly accessible data. The initial files spanned various spatial resolutions (10 m, 12.5 m, and 0.25°), which were all resampled physically to a 30 m resolution using bilinear interpolation. 30 m is the coarsest resolution available among the datasets, ensuring compatibility among various layers while reducing interpolation errors. This harmonious balance between accuracy helped the computational analysis to be done at a city-scale with sufficient spatial detail. However, it was also apparent that this resampling inevitably smoothed the finer-scale topographic variation, which was a limitation of this approach. Predictors, such as E, As, AR, LULC, So, TWI, DTR, NDVI, NDBI, NDWI, and TPI, were reclassified using natural breaks, and Cu used human reclassification techniques.

2.3.2.2. Multicollinearity

Multicollinearity refers to the presence of a linear relationship among independent variables [38]. Conducting a multicollinearity test is essential when multiple independent factors are considered. if unaddressed, multicollinearity can produce misleading results by inflating standard errors and reducing the statistical significance of individual predictors [39]. To describe the multicollinearity tolerance, the variance inflation factor (VIF) was computed using the following equation.

$$\text{Tolerance } = 1 - R_j^2 \tag{1}$$

$$V\mathbb{F} = \frac{1}{1-R_j^2} \tag{2}$$

$$\text{Condition Index } = \sqrt{\frac{\text{Largest Eigenvalue}}{\text{Smallest Eigenvalue}}} \tag{3}$$

Multicollinearity issues occur when the VIF exceeds 10 and the tolerance value falls below 0.10 [40]. In addition to VIF and tolerance, Condition Index (CI) was another statistical metric used in this study (Eq. 3). CI was used to assess multicollinearity across the model, not just individual predictors [41]. High CI (>30) values indicated potential collinearity problems. The tolerance value exceeding 0.10 and the VIF value below 10 for each factor influencing flash floods ($p < 0.01$, $p < 0.05$) indicated the absence of collinearity among these factors.

2.3.3. Analytical Hierarchical Process (AHP)

The MCDM approach can rationally address this issue, as it is evaluated based on multiple criteria. The AHP approach, a Multi-Criteria Decision Method (MCDM), described by Saaty, was implemented in this study [42]. It utilizes a preference matrix to establish priority among the components by comparing alternatives in pairs. AHP is comprised of three major processes: (i) Determining the proportional relevance of components and matrix development via pairwise comparison; (ii) allocating criteria weights using the Saaty scale (Table 2); and (iii) estimating the consistency ratio (CR).

Table 2. Pairwise comparison scale by Saaty [42].

Score	Preference	Explanation
1	Equally favour	Both factors are equally favoured
3	Moderately favour	One factor is slightly preferable to others
5	Strongly favour	One factor is strongly favourable than the other
7	Very strongly favour	One factor is very strongly preferred over the other
9	Extremely favour	One factor is extremely favoured over the other
2, 4, 6, 8	Intermediate	Placed the weight between 1, 3, 5, 7, and 9

2.3.3.1. Development of a pairwise and standardized comparison matrix

As twelve parameters were selected for Urban Flood Susceptibility Zones (UFSZ), a pairwise comparison matrix of order 12 was developed (shown in Table 3), evaluating twelve parameters (C1, C2, C3, C4, C5, C6, …, and C12) against each other. For instance, when parameters C1 (elevation) and C2 (LULC) were directly compared, parameter C1 was regarded as of considerable importance (7), while the other parameter was assigned equivalent relative weight. The reciprocal of 1/7, or 0.14, was promptly used in the transposed position. Similarly, all parameters were compared pairwise and scored between 1 (equal importance) to 9 (extremely more important).

In this study, the pairwise comparisons were performed through a combination of literature review and structured expert consultation. The expert team consisted of a hydrologist specialized in urban drainage, a BDA urban planner, and a geospatial consultant on RS-GIS. Each of them, using their specialized knowledge, provided independent pairwise preferences. A consensus-building discussion was then held, and all differences were resolved, ensuring final judgements should reflect science-based rigor and local urban planning context. This offered an adequate foundation to develop the pairwise comparison matrix provided in Table 3 while keeping individual biases to a minimum.

Table 3. Pairwise comparison matrix for flood susceptibility.

	E	LULC	DTR	NDBI	NDVI	NDWI	So	AR	TWI	TPI	As	Cu	Priority vector (PV)	Weight (%)
E	1	7	3	3	3	7	7	8	9	9	9	9	0.25	25%
LULC	0.14	1.00	8	3	3	4	6	7	8	8	8	9	0.19	19%
DTR	0.33	0.13	1.00	3	3	4	6	7	8	9	8	9	0.15	15%
NDBI	0.33	0.33	0.33	1.00	3	3	5	5	5	5	7	8	0.11	10%
NDVI	0.33	0.33	0.33	0.33	1.00	3	5	5	5	7	9	9	0.10	9%
NDWI	0.14	0.25	0.25	0.33	0.33	1.00	3	3	5	7	7	7	0.06	7%
So	0.14	0.17	0.17	0.20	0.20	0.33	1.00	3	3	5	7	7	0.05	5%
AR	0.13	0.14	0.14	0.20	0.20	0.33	0.33	1.00	3	3	5	5	0.03	3%
TWI	0.11	0.13	0.13	0.20	0.20	0.20	0.33	0.33	1.00	3	5	5	0.03	3%
TPI	0.11	0.13	0.11	0.20	0.14	0.14	0.20	0.33	0.33	1.00	3.0	3	0.02	2%
As	0.11	0.13	0.13	0.14	0.11	0.14	0.14	0.20	0.20	0.33	1.00	3	0.01	1%
Cu	0.11	0.11	0.11	0.13	0.11	0.14	0.14	0.20	0.20	0.33	0.33	1	0.01	1%
Sum	**3.00**	**9.84**	**13.70**	**11.73**	**14.30**	**23.29**	**34.15**	**40.07**	**47.73**	**57.67**	**69.33**	**75**	**$\sum = 1$**	**100%**

The subsequent step involved normalization of the matrix by dividing each element by the sum of its respective column, ensuring all factors were on a standard scale [43] (Eq. 4). The Priority vector, representing the influencing weight of parameters, was then calculated using the geometric mean of each row (Eq. 5) [44]. To check consistency, the principal eigenvalue (λmax) was estimated by multiplying the original matrix by the priority vector and averaging the ratio of each resulting element to its corresponding weight (Eq. 6) [45]. This eigenvalue indicated the reliability of the derived weights [46].

$$W_i = \frac{\sum_{i=1}^{n} \left[\frac{Ci}{\sum_{i=1}^{n} Ci}\right]}{n} \quad (4)$$

$$C_j = \frac{\sum_{i=1}^{n} [Ci \times Wi]}{Wi} \quad (5)$$

$$\lambda_j = \frac{\sum Cj}{n} \quad (6)$$

2.3.3.2. Calculating the consistency ratio

To ensure the reliability of the pairwise comparison matrix, the consistency ratio (CR) was calculated. First, the consistency index (CI) was computed using the formula: CI = (λmax – n)/(n – 1), where λmax was the principal eigenvalue and n was the number of criteria (Eq. 7). Next, CR was derived by dividing the CI by the Random Index (RI) corresponding to the number of criteria (Eq. 8). The RI values, proposed by Saaty (1980), are listed in Table 4. A CR value ≤ 0.1 indicates acceptable consistency, while a value > 0.1 suggested the need to revise the pairwise judgments [47].

Table 4. Random Index (RI) to check Consistency Ratio for a varied matrix

1	2	3	4	5	6	7	8	9	10	11	12	13	14	15
0.00	0.00	0.58	0.90	1.12	1.24	1.32	1.41	1.45	1.49	1.51	1.48	1.56	1.57	1.59

$$CI = \frac{\lambda max - n}{n - 1} \quad (7)$$

$$CR = \frac{CI}{RI} \quad (8)$$

2.4. Mapping of urban flood susceptibility zonation (UFSZ)

The Urban flood susceptibility zonation (UFSZ) map was generated using the Urban flood susceptibility index (UFSI) values obtained from Eq. 9.

$$\text{UFSI} = \sum_{i=1}^{n} \text{Wi} \times \text{Ri} \quad (9)$$

where Wi is the weight of the individual flood influencing criteria and Ri is the rating of the sub-class. Subsequently, all twelve thematic layers were combined in a GIS environment through weighted overlay analysis, and the UFSZ was obtained. Finally, the map was categorized into five zones utilizing the Natural Break classification (Jerks) method within a GIS environment. The five categories were defined as follows: Very low (0.06–0.14), low (0.15–0.22), medium (0.23–0.27), high (0.28–0.32), and very high (0.33–0.43).

2.5. AUC and ROC analysis

The reliability of the Urban flood susceptibility zonation (UFSZ) was evaluated using the Receiver Operating Characteristic (ROC) curve and the Area Under the Curve (AUC), which are widely recognized methods for validating spatial prediction models [48]. The ROC curve was constructed by plotting sensitivity (true positive rate) against 1-specificity (false positive rate), derived from eqs. (10) and (11):

$$x = 1 - \text{ specificity } = 1 - \left[\frac{\text{TN}}{(\text{TN} + \text{FP})}\right] \tag{10}$$

$$y = \text{ sensitivity } = \left[\frac{\text{TN}}{(\text{TP} + \text{FN})}\right] \tag{11}$$

where TN = True negative, TP = true positive, and FP = false positive.

To compute AUC, the flood inventory data (Figure 3) was randomly divided into 70% training and 30% testing datasets. The success rate was calculated using the training data, while the prediction rate was assessed using the testing data. An AUC value less than 0.50 indicates poor model performance, whereas a value closer to 1 indicates strong predictive capability [49]. A model is generally considered acceptable if it achieves an AUC greater than 0.70 [50]. In this study, AUC calculations were performed using the Arc Sum function in ArcGIS 10.4.

2.6. Validation of UFSZ

We emplouyed the Google Earth Engine (GEE) as a cloud-based geospatial analysis platform to detect and validate urban flood events on a real-time basis for the BMC region. Floods were detected using Sentinel-1 synthetic aperture radar (SAR) imagery, a data source with all-weather and day-night imaging capabilities [51]. The specified methodology consisted of data acquisition, data preprocessing, and flood detection with a clear objective of determining the extent of the area affected by the flood using Sentinel-1 SAR imagery, which was used to assess the regions acquired from the SAR images from the COPERNICUS/S1_GRD dataset wherein floodwaters was best detected by VH-polarized backscatter intensity in Interferometric Wide Swath (IW) mode, which increased the probability of waterbody detection by minimizing surface roughness effects [52,53]. To avoid the probability of false detections, images taken before and after the flood (June 25–July 10, 2023, July 15–25, 2023) were selected with temporal alignment of observed events (field survey) to improve the overall reliability of the results. Each image set was clipped to the Region of Interest (ROI) to eliminate data outside the study area.

Flood detection was performed by computing the difference in radar backscatter between pre- and post-flood conditions. Given that inundated areas exhibited lower backscatter due to the specular reflection of radar signals over smooth water surfaces [54], the mean backscatter intensity for both periods was calculated, and a flood difference map was generated using Eq. 12:

$$FD = \bar{\sigma}^0_{\text{Post-flood}} - \bar{\sigma}^0_{\text{Pre-flood}} \tag{12}$$

where FD represents the flood difference, and $\bar{\sigma}^0$ denotes the mean radar backscatter intensity. For flood detection, negative FD values are considered, since smooth water surfaces are assumed to have low values of backscatter due to specular reflection [55]. Additionally, unlike others that have used only empirical methods, we used Otsu's thresholding technique to automate and dynamically determine the best threshold for classification of the flood.

Otsu's algorithm calculates a statistically optimal separation between flooded and non-flooded pixels by maximizing inter-class variance in the FD image histogram [56]. Moreover, to avoid overestimation of flood extent, the permanent water bodies were masked using the JRC Global Surface Water dataset, effectively eliminating rivers, lakes, and other permanent water bodies from flood classification. However, the problem of classification accuracy remained because the process failed to identify mixed pixels in vegetated and urbanized areas. To reduce noise, a connected pixel filter was applied, retaining only flood patches with ≥10 connected pixels, which significantly improved the reliability of the results. The final outputs included a binary flood map (1 = flood, 0 = no flood) [57].

3. Results and discussion

3.1. Multicollinearity diagnostics

The independent variables' multicollinearity diagnostics were assessed using the Condition Index (CI), Variance Inflation Factor (VIF), and Tolerance values, as shown in Table 5. These metrics help analyze the dependence relations among the predictors and their impact on regression analysis. Key metrics used to measure the extent of problematic multicollinearity conditions include a VIF value greater than 5 (VIF ≥ 10, which indicates severe conditions) and a tolerance value closer to zero [58]. According to the study model, it was established that predictors E, TWI, NDWI, NDVI, As, DTR, AR, and So attained the requisite significance threshold of 0.05 (p-value, Sig. $p < 0.05$) and established themselves as significant predictors. In contrast to the aforementioned, the predictors Cu, TPI, and LULC had p-values (>0.05), which suggests the insignificance of these predictors in the model. In the context of this study, the CI, a measure of multicollinearity, derived from the eigenvalues of the scaled correlation matrix, suggests strong multicollinearity if CI is >30 [59]. In this study, while most predictors had CI values below this threshold, NDVI, NDWI, and NDBI registered VIF of 4.47, 3.04, and 3.12, respectively, alongside low tolerance values of 0.04, 0.05, and 0.32. Extremely low CI values on the scale of tolerance signifies that substantial amounts of variance in these variables are explained in relation to other predictors within the model, thereby reinforcing the presence of moderate multicollinearity.

Specifically, the variable NDVI had the highest VIF within a proximity of a widely recognized threshold for significant collinearity concerns, which was five [60]. This is consistent with other works where vegetation indices, alongside NDVI and NDWI, tend to correlate strongly due to overlapping spectral information and shared sensitivity to surface characteristics, such as vegetation cover and water content [61]. Additionally, the moderate VIF for NDBI could be explained by its association with NDVI and NDWI, as such spectral indices tend to represent different facets of the interrelated and complex land surface conditions [62]. Even though there was moderate collinearity among NDVI, NDBI, and NDWI, each of the indices represents unique surface characteristics that directly influence runoff and infiltration patterns. Their incorporation is what makes the susceptibility model realistic in regard to capturing the intricate land surface interactions in Bhubaneswar. Additionally, the AHP-derived weights remained stable, and the zonation output of the susceptibility was not significantly influenced by these moderate correlations, indicating the robustness of the weighting process. Even though Principal Component Analysis (PCA) is extensively covered in the literature as a means of dimensionality reduction to resolve collinearity, it was not done in this case. Nevertheless, in future investigations, researchers might consider employing PCA or some other statistical methodologies with a view to further determining the robustness of multicollinear variables. In addition, E (CI = 1.00; VIF = 1.01) exhibited high tolerance and low VIF values, suggesting minimal multicollinearity and its (i.e., E's) potential use as independent predictors in the model.

Table 5. Multicollinearity results among predictor variables.

Sl. No.	Variables	Condition Index	Sig.	Collinearity Statistics	
				Tolerance	VIF
1	E	1.00	0.00		
2	NDBI	2.22	0.16	0.32	3.12
3	TWI	2.82	0.00	0.77	1.28
4	TPI	4.64	0.82	0.54	1.84
5	NDWI	4.81	0.00	0.32	3.04
6	NDVI	5.32	0.01	0.22	4.47
7	Cu	7.29	0.54	0.60	1.65
8	As	1.80	0.00	0.98	1.01
9	DTR	4.29	0.00	0.92	1.08
10	AR	1.24	0.00	0.89	1.12
11	So	6.52	0.00	0.90	1.10
12	LULC	3.83	0.88	0.84	1.18

3.2. Identification of flood influencing thematic layers

Elevation is a key factor in controlling the flow of floods, their direction, and the level of submerged water depth [48]. Alos Palsar DEM was used to generate elevation maps for the area (Figure 4a), indicating that the southern and southeastern parts of the city have the lowest elevation and, therefore, are more likely to be affected by urban flooding. The orientation of a slope on the earth's surface is referred to as the aspect. It significantly regulates the convergence and trajectory of surface water flow [63]. Figure 4 b shows the aspect of the study area, indicating that the north and northwestern parts have a higher slope orientation compared to the rest of the area. Another significant component in assessing the intensity of a flash flood is curvature, which denotes the earth's shape.

This component has a crucial function in controlling surface water flow and the infiltration process. In this study, the curvature map (Figure 4c) of interest is categorized into five classes, where negative values indicate a concave slope and positive values depict a convex slope. Concave terrains are more likely to experience water accumulation, and the distance to the river plays a vital role in urban flood inundation mapping [64].

TPI and TWI (Figure 4d and 4e) are terrain-derived parameters and significantly influence surface runoff. Areas with lower TPI scores and higher TWI values are often seen as susceptible to flash floods [65]. We also regarded the soil type as a relevant criterion since soil type (Figure 4f) directly affects infiltration and groundwater recharge and rain erosivity [66]. According to the literature review, precipitation volume significantly influences flood development. The annual average precipitation (Figure 4g) for the study area from 2022 to 2023 was sourced from the IMD Database. The closer the river/stream is, the more likely the urban areas are to be affected by the flood [67]. In this study, the value of DTR (Figure 4h) ranges from 0 to 2101 m. Areas with lower values are more likely to be flooded, whereas regions with higher values are farther from the river/stream. LULC, NDWI, NDBI, and NDVI (Figure 4i-l) are the major factors that affect the occurrence of floods and have an impact on the surface runoff, as well as the soil storage water capacity [68]. For the following AHP method, all the parameters selected above were converted to a raster grid with 30 m × 30 m cells.

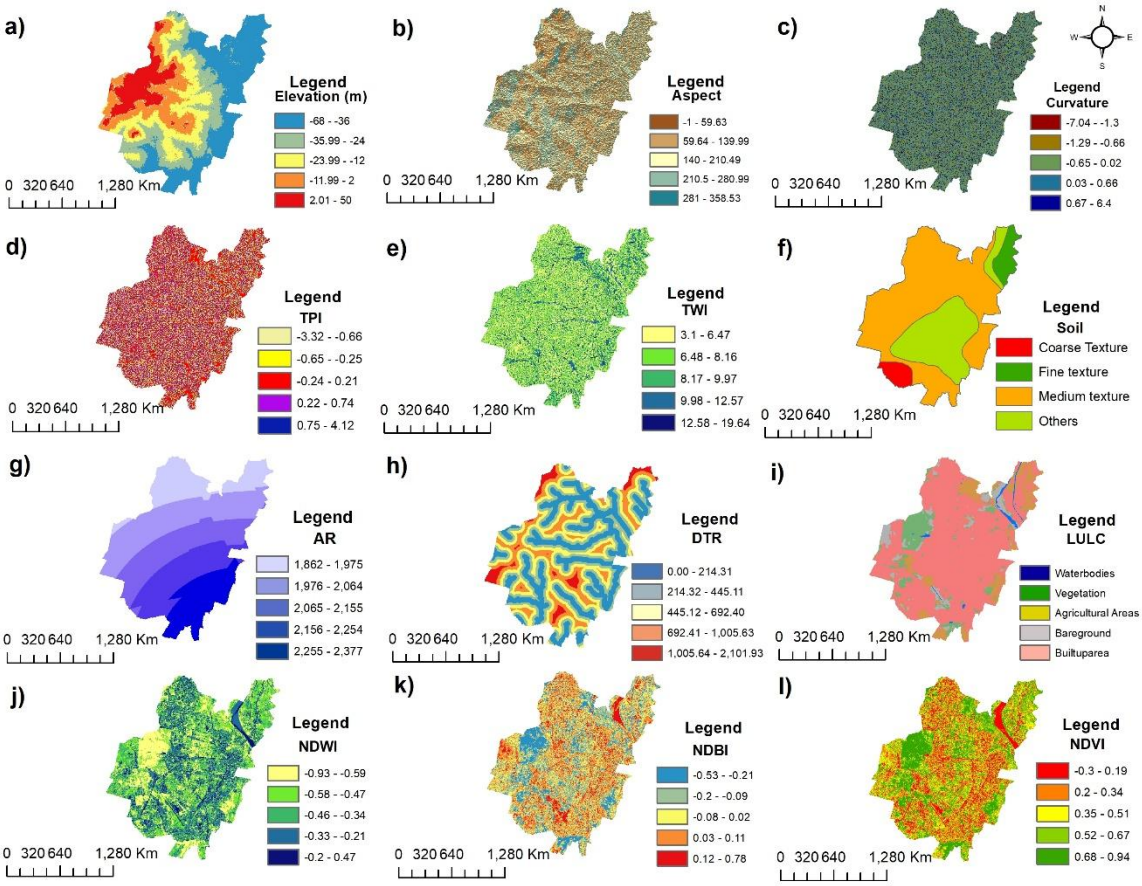

Figure 4. Factors Influencing Urban Flooding. (a) Elevation, (b) Aspect, (c) Curvature, (d) TPI, (e) TWI, (f) Soil, (g) Annual Rainfall, (h) DTR, (i) LULC, (j) NDWI, (k) NDBI, and (l) NDVI.

3.3. Urban flood susceptibility mapping ranking of layers by AHP

Based on the AHP technique, the relative weights of influencing parameters were computed in percentages, and the consistency ratio (CR) was calculated as 0.06 (a CR value of 0.10 or less was considered relevant) (Table 6). The CR value demonstrated a respectable level of accuracy in the pair-wise comparison matrix. Furthermore, the thematic layers of each parameter were classified into five classes using the reclassify function of ArcMap. Table 7 illustrates the relative significance of each component and its subfactors in the research. Our findings indicated that elevation (0.25, 25%) is the predominant factor in identifying zones prone to flash floods. The second influencing factor is LULC (0.19, 19%). Within the subfactors of the LULC thematic layer, the built-up area emerged as the most significant subfactor (in identifying regions prone to flash floods). This built-up land occupies most of the study area, covering 107.07 square kilometers, and these urbanized zones, particularly roads and structures, significantly impact hydrological processes. Moreover, urbanized areas substantially influence infiltration capacity and surface runoff. The infiltration capacity is often considerably diminished by these developed regions, resulting in increased surface runoff. Consequently, the LULC factor after elevation might be considered the most critical determinant of places susceptible to flash floods. Following LULC, DTR at 0.15 (15%), NDBI, NDVI, NDWI, and Soil type emerged as the subsequent significant criteria, each contributing substantially to the susceptibility of places prone to flash floods. In [69], the researchers selected LULC, slope, curvature, and TWI as the major criteria

for creating a flash flood susceptibility map. In the research, Cu (0.01,1%), As (0.01,1%), TPI (0.02,2%), and TWI (0.03,3%) were shown to be the least impacted parameters. All these parameters had little effect on the development of the flood susceptibility map for the research region. This was likely attributable to the reduced surface area occupied by these indicators in the study area. Each parameter's raster layer in grid format was multiplied by its assigned weight using Eq. 9, and the arithmetic weighted sum overlay technique in the ArcGIS 10.9 software was utilized to integrate these weighted parameters into a comprehensive flood hazard map. Small values denoted low susceptibility to floods, and high values denoted high susceptibility to floods.

Table 6. Consistency check of the aggregated data for flood susceptibility mapping.

Lambda max	N	CI	CR
13.05	12	0.09	0.06

Table 7. Weight assignment to each component and sub-factor.

Parameter	Criteria Weight (Wi)	Class	Range	New Level	Area (km^2)	Area (%)	Sub-criteria weight (Ri)
Elevation (-)	0.25	1	−68.00 to −36.00	Very High	49.03	33.68	0.51
		2	−35.99 to −24.00	High	29.29	20.12	0.26
		3	−23.99 to −12.00	Medium	27.18	18.67	0.13
		4	−11.99 to 2.00	Low	23.81	16.36	0.06
		5	2.01 to 50.00	Very Low	16.22	11.14	0.04
Aspect (+)	0.01	1	−1.00 to 59.63	Very Low	42.46	29.17	0.06
		2	59.64 to 139.99	Low	34.79	23.90	0.09
		3	140.00 to 210.49	Medium	23.23	15.96	0.15
		4	210.50 to 280.99	High	24.26	16.67	0.26
		5	281.00 to 358.53	Very High	20.81	14.30	0.44
Curvature (-)	0.01	1	−7.04 to −1.30	Very High	1.85	1.27	0.50
		2	−1.29 to −0.66	High	20.12	13.83	0.26
		3	−0.65 to 0.02	Medium	74.59	51.24	0.14
		4	0.03 to 0.66	Low	26.99	18.54	0.07
		5	0.67 to 6.40	Very Low	22.00	15.12	0.04
Soil Texture (+)	0.05	1	Coarse	Very Low	5.19	3.66	0.05
		2	Fine	Low	7.08	4.95	0.09
		3	Medium	Medium	92.86	63.55	0.15
		4	All other Value (DESCR)	High	35.91	24.65	0.26
		5	Others (Water bodies, River Bed)	Very High	4.51	3.19	0.45
LULC (+)	0.19	1	Water Bodies	Medium	1.48	1.13	0.14
		2	Vegetation	Very Low	12.99	8.99	0.04
		3	Agricultural Areas	High	15.02	10.38	0.26
		4	Bare ground	Low	9.14	6.36	0.06
		5	Built-up Area	Very High	106.90	73.14	0.50

Continued on next page

Parameter	Criteria Weight (Wi)	Class	Range	New Level	Area (km^2)	Area (%)	Sub-criteria weight (Ri)
NDVI (-)	0.10	1	−0.30 to 0.19	Very High	24.30	16.71	0.43
		2	0.20 to 0.34	High	29.17	20.05	0.26
		3	0.35 to 0.51	Medium	29.19	20.06	0.15
		4	0.52 to 0.67	Low	32.23	22.13	0.10
		5	0.68 to 0.94	Very Low	30.65	21.05	0.06
NDWI (+)	0.06	1	−0.93 to −0.59	Very Low	32.29	22.17	0.06
		2	−0.58 to −0.47	Low	38.97	26.74	0.10
		3	−0.46 to −0.34	Medium	30.99	21.28	0.16
		4	−0.33 to −0.21	High	30.40	20.88	0.26
		5	−0.20 to 0.47	Very High	12.80	8.93	0.42
NDBI (+)	0.11	1	−0.53 to −0.21	Very Low	19.79	13.64	0.06
		2	−0.20 to −0.09	Low	34.00	23.34	0.10
		3	−0.08 to 0.02	Medium	39.29	26.96	0.15
		4	0.03 to 0.11	High	36.47	25.03	0.26
		5	0.12 to 0.78	Very High	15.98	11.03	0.43
Distance to River (-)	0.15	1	0.00 to 214.31	Very High	43.78	30.03	0.42
		2	214.32 to 445.11	High	38.21	26.22	0.26
		3	445.12 to 692.40	Medium	34.53	23.71	0.16
		4	692.41 to 1005.63	Low	22.64	15.59	0.10
		5	1005.64 to 2101.93	Very Low	6.35	4.45	0.06
Annual Rainfall Intensity (+)	0.03	1	1862 to 1975	Very Low	24.61	16.93	0.05
		2	1976 to 2064	Low	39.73	27.26	0.09
		3	2065 to 2155	Medium	30.96	21.26	0.15
		4	2156 to 2254	High	27.74	19.06	0.26
		5	2255 to 2377	Very High	22.50	15.49	0.45
TPI (-)	0.02	1	−3.32 to −0.66	Very High	19.02	13.25	0.49
		2	−0.65 to −0.25	High	32.86	22.56	0.26
		3	−0.24 to 0.21	Medium	49.14	33.64	0.14
		4	0.22 to 0.74	Low	29.04	19.95	0.07
		5	0.75 to 4.12	Very Low	15.30	10.60	0.04
TWI (+)	0.03	1	3.10 to 6.47	Very Low	49.60	34.08	0.05
		2	6.48 to 8.16	Low	44.53	30.59	0.09
		3	8.17 to 9.97	Medium	29.06	19.97	0.15
		4	9.98 to 12.57	High	17.99	12.36	0.26
		5	12.58 to 19.64	Very High	4.37	3.00	0.45

3.4. Urban flood susceptibility zonation

A flood susceptibility map was generated using twelve mapping parameters, resulting in five separate classes (zones) (Figure 5). The region exhibited very low, low, moderate, high, and very high susceptibility to flood threats, comprising 8.21%, 18.81%, 27.13%, 29.38%, and 16.44% of the total area, respectively (Table 8). Generally, regions susceptible to flood dangers and locations with significant runoff are the results of the diverse array of contributing elements. Analysis revealed a heterogeneous distribution of flood zonation across the BMC region, where the intensity of zonation

varies according to variation in its determinant factors. High flood risk zones are mostly in the southern, partially in the northern, and southeastern regions, while moderate flood risk regions are in the central section of the research area. Areas exhibiting little and negligible flood risk are mostly in the northwest, southwest, and western regions (Figure 5).

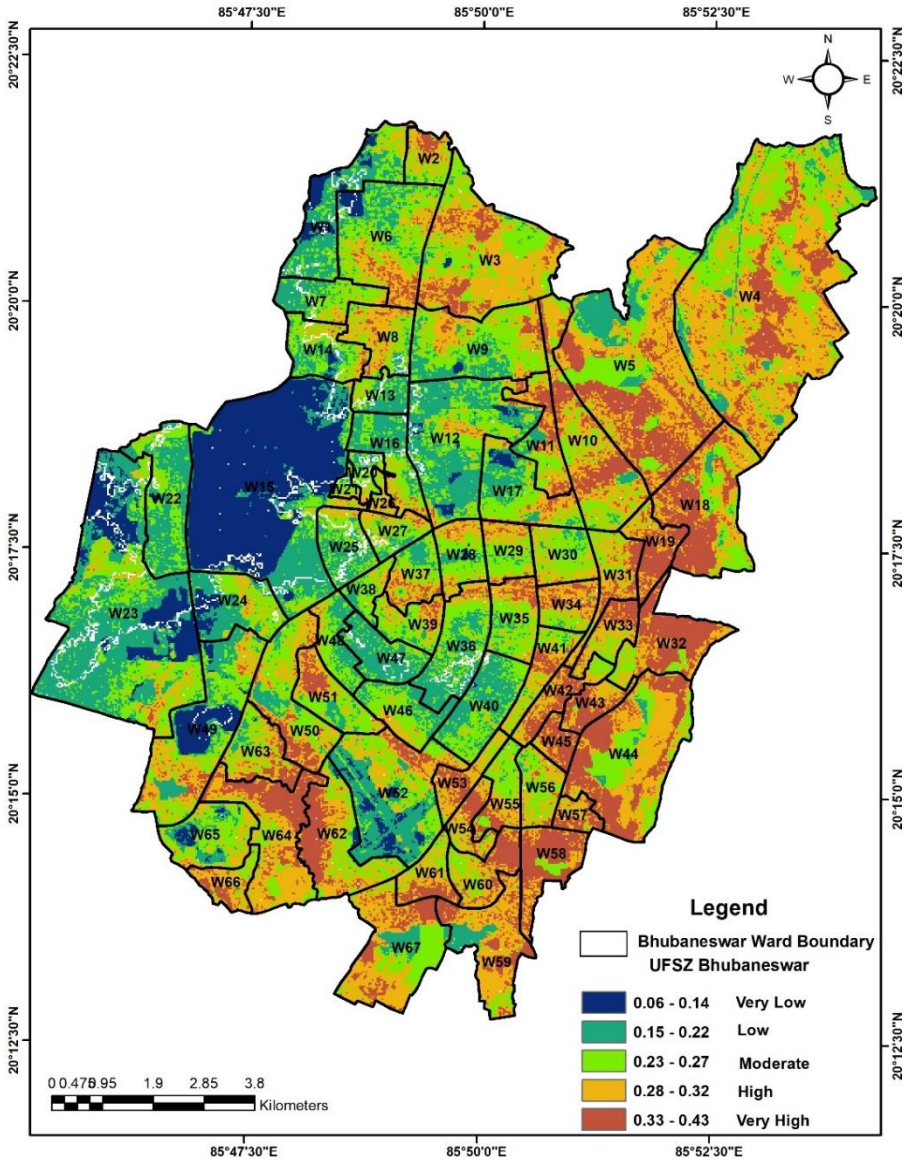

Figure 5. Urban flood susceptible Zonation for BMC.

Locations designated as having "high susceptibility" were characterized by features such as lower Digital Elevation Model (DEM) values, slope, and Proximity to rivers, which enhance susceptibility to flood risks. In the central region of the area, the presence of moderate elevation and probably well covered stormwater drainage system partially reduces flood susceptibility, but high built-up presence and moderate proximity to natural drainage could cause occasional flooding events. Conversely, the western and northwestern areas have minimal flood danger owing to their high DEM Values, which reduce the impact of most rainfall, while dense vegetation cover further mitigates runoff and enhances water absorption. These areas' lesser proximity to the river can also be attributed to their zonation as less suspectable regions. Furthermore, the analysis showed that high-susceptibility zones in the southern and central parts of Bhubaneswar overlap with dense built-up areas, informal settlements, and key transport

corridors. This indicated that flood risks are not only driven by environmental factors but also intersect with critical urban functions. Recognizing these overlaps is essential for planning drainage upgrades, prioritizing resilient infrastructure, and identifying potential locations for flood shelters.

Table 8. Urban flood susceptibility status of the BMC region.

Sl. No.	Urban flood susceptible zones	Area in Km^2	Percentage
1	Very low	11.95	8.21
2	Low	27.38	18.81
3	Moderate	39.50	27.13
4	High	42.76	29.38
5	Very High	23.94	16.44
	Total =	**145.55**	**100**

3.5. Validation of model performance

The assessment of the flood susceptibility model was carried out using ROC curve analysis, as shown in Figure 6, which is widely used in flood risk studies for evaluating flood susceptibility models' performance. According to the AUC reached by the model, which was 0.87, the model could differentiate susceptible from non-susceptible regions with quite good accuracy. To set a benchmark of model performance, AUC was compared against the tiered classification thresholds: AUC < 0.7 (poor), 0.7 ≤ AUC < 0.8 (fair), 0.8 ≤ AUC < 0.9 (good), and AUC ≥ 0.9 (excellent model). Thus, the AUC obtained, which was 0.87, corresponded to the "good" standard, which served to further validate the AHP-based susceptibility model. Values of AUC near 1.0 was an indicator of outstanding predictive ability. AUC values above 0.8 were normally taken to signify a model with acceptable performance [70]. The ROC curve capturing the performance of the model was well above the diagonal random guessing line, serving to further confirm the model's well established reliability in performance. Thus, the predictive ability was very high, which suppoerted the inclusion of geo-spatial and socio-environmental components in the flood susceptibility analysis and aligns with the conclusions of more recent works [71]. This implied that the model can assist decision makers in the determination of regions that are potentially flood affected areas in planning of resource allocation and subsequent disaster management measures.

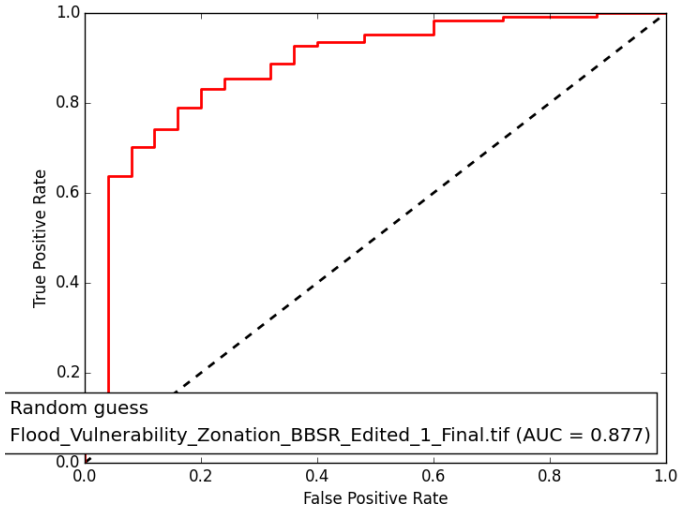

Figure 6. AHP Model validation using AUC.

The observed AUC value of 0.87 was corroborated by previously conducted AHP-based geospatial models. In these studies, AUC values ranged from 0.80 to 0.90 [72]. This underlines the confirmed efficacy of the methodology adopted in urban flood susceptibility assessments, especially in rapidly growing urban areas such as Bhubaneswar. This also strengthens the rationale for practical application as well as provide solid foundation for future research.

3.6. Flood zonation validation using GEE

The flood detection analysis using GEE-based Sentinel-1 SAR data provided a comprehensive understanding of the flood extent and severity within the BMC region. The derived maps, Before Flood, After Flood, Flood Severity Map, and Flood Binary Map, offer critical insights into the spatial distribution and severity of the flood event. The "Before Flood" and "After Flood" (Figure 7a, b) maps highlight the temporal dynamics in surface water distribution before and after the flood event.

The post-flood map (Figure 7b) shows the extent of flooding, with darker areas that signify open water or areas that are submerged, notably along the banks of the Kuakhai and Daya Rivers and regions of lower elevation within the city. The significant change in radar backscatter intensity, as observed in both images (Figure 7a, b), indicates the degree to which the area has sustained damage from the flooding. Post-flood image recorded reduced backscatter values compared to the pre-flood situation due to the specular reflection of the radar signal by the inundated regions. Figure 7a shows the VH backscatter composite images taken before the floods, where the built-up and vegetated areas have scattered brighter values. Conversely, rivers and water bodies are represented in darker tones attributed to their low reflectivity. Figure 7b shows backscatter images taken after floods, highlighting areas of reduced reflectance value attributed to water inundation.

Notably, clusters of reduced VH intensity can be seen in the northeastern, southeastern, and southwestern parts of BMC. The "Flood Severity Map" (Figure 7c) shows backscatter differences (ranging from −18.42 dB to +3.2 dB) that are color-coded into four classes. The darkest tones correspond to regions of significant backscatter drop, indicating severe flooding. The map is derived from the difference in radar backscatter before and after flooding (Eq. 12). The negative backscatter values in the post-flooding map indicate the increased water presence as backscatter reduction becomes greater. The observed spatial pattern indicates that most of the flooding is along the drainage channels, low lying areas, and peri urban settlements, which is consistent with the known areas of flooding identified by BMC. The "Flood Binary Map" (Figure 7d) shows the outcome of a categorical classification of the landscape differentiating flooded and non-flooded zones using the optimal Otsu's threshold, subsequently refined by excluding permanent water bodies and small pixels clusters. This method of classification provides accurate flood extent mapping and aligned well with historical flood records, reinforcing the reliability of the methodology.

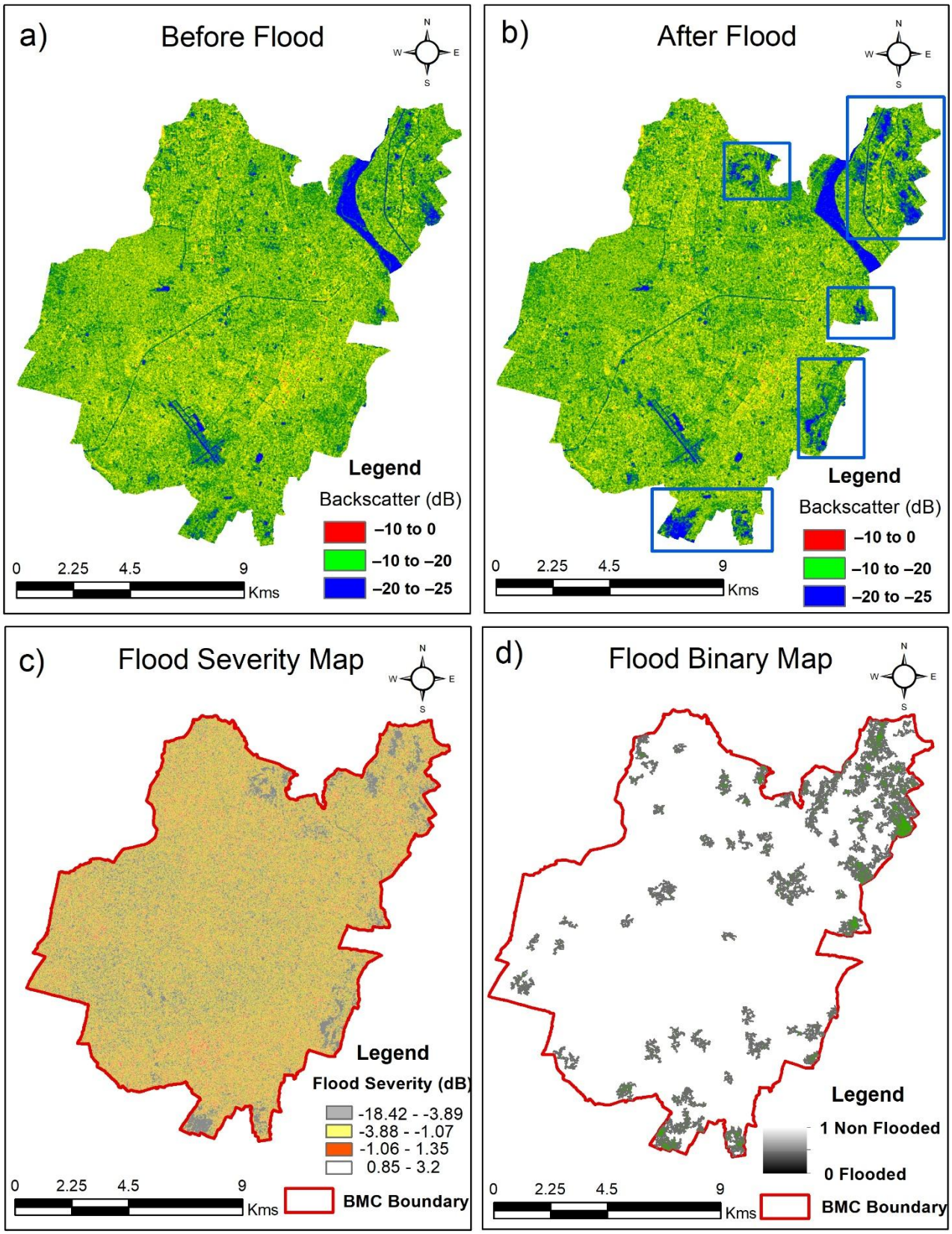

Figure 7. Urban Flood Analysis Using Google Earth Engine (GEE). (a) Pre-Flood Image, (b) Post-Flood Image, (c) Flood Severity Map, and (d) Flood Binary Map (Flooded and Non-Flooded Areas).

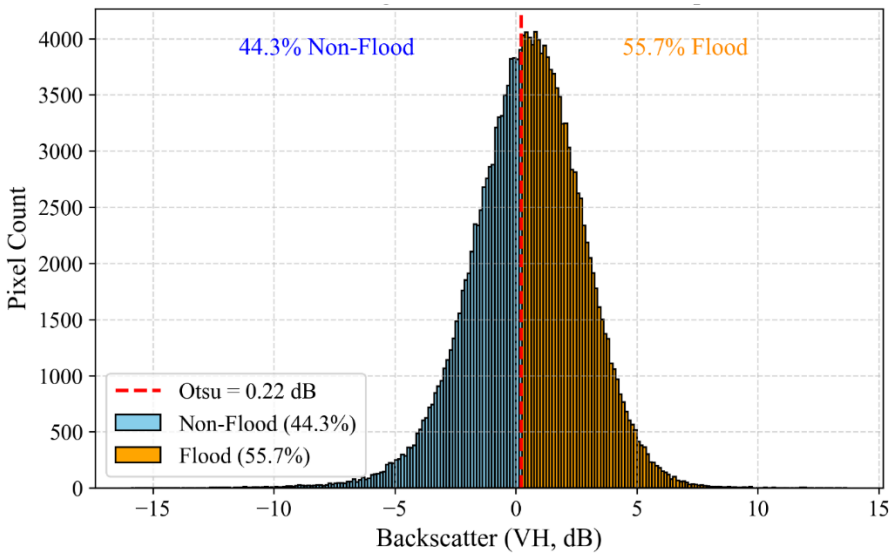

Figure 8. Pixel distribution of VH backscatter values with an Otsu-derived threshold split.

The histogram displaying the VH backscatter values and the Otsu's method-derived threshold histogram split can also be seen in Figure 8. The threshold value of 0.22 dB successfully partitions the pixel population into two categories: Flooded (55.70%) and non-flooded (44.30%). Most of the pixels were below the threshold value, representing inundated areas with relatively low backscatter due to specular reflection. Automated thresholding flood mapping provides a more objective approach and is more reproducible than manual flood mapping.

3.6.1. Cross-Validation of SAR flood extent with flood susceptibility map

To assess the spatial correspondence between the flood susceptibility map and observed flood extent, Sentinel-1 SAR-derived flood data for the study area were overlaid on the rasterized susceptibility classes. The total flooded area identified from SAR imagery was 7.05 km², distributed across vulnerability classes, as summarized in Table 9.

Table 9. Cross-validation of the SAR-derived flooded area with UFSZ.

Vulnerability Class	Flooded Pixels	Flooded Area (ha)	Flooded Area (km2)	Percentage (%)
Very Low	120	10.81	0.10	1.53
Low	1093	98.37	0.98	13.95
Moderate	2541	228.69	2.28	32.44
High	3107	279.63	2.79	39.66
Very High	973	87.57	0.87	12.42
Total	**7834**	**705.06**	**7.05**	**100**

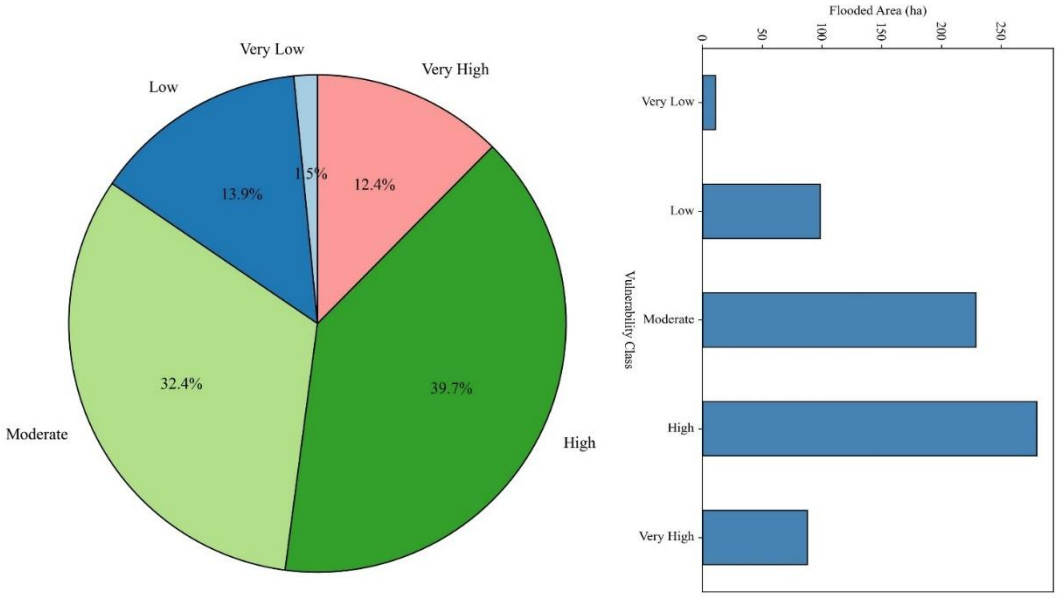

Figure 9. Pixel distribution of VH backscatter values with an Otsu-derived threshold.

From Figure 9, which illustrates results, it is evident that more than half the flooded area (52.08%) coincided with the High and Very High susceptibility classes, confirming that areas identified as highly vulnerable in the UFSZ map are prone to inundation. Furthermore, only 15.48% of the flooded area fell within "Low" and "Very Low" susceptibility zones, indicating minimal false positives. This cross-validation demonstrated a strong spatial agreement between the SAR-observed flood extent and the proposed flood susceptibility classification, thereby supporting the reliability of the susceptibility mapping methodology.

3.7. Comparison with hazard and risk maps

To further evaluate the accuracy of the generated susceptibility map, the maps were compared with the Hazard Risk and Vulnerability Analysis (HRVA) flood maps of the city of Bhubaneswar, as well as the Odisha State Disaster Management Authority (OSDMA) flood hazard maps. The comparison indicated that more than 80% of the areas classified as "High" and "Very High" in this study are spatially aligned with areas of high risk and are flood-prone in the government hazard maps. This further confirms the efficacy of the AHP-based framework and demonstrated its comparative superiority over conventional methods of hazard delineation while offering greater spatial detail (30 m resolution compared to 100 m in the OSDMA maps).

3.8. Comparative analysis with similar studies

Several prominent flood susceptibility studies across India demonstrated strong methodologies but differed in validation approaches. For instance, the Western Ghats study achieved an AUC of 0.84 using diverse environmental and socio-economic layers [73], while the Idukki district (AUC = 0.91) and Subarnarekha basin (AUC = 0.93) models relied on AHP-based frameworks with expert inputs [74,75]. For the Chalakudy basin study, the researchers also incorporated Sentinel-1 SAR validation, though without an explicit AUC [76]. In contrast, this Bhubaneswar study delivers a high predictive accuracy (AUC = 0.87), 30 m spatial resolution, and strengthens model credibility through SAR-based flood extent overlay validation, with over 52% of observed floods falling into the "High" or "Very High"

susceptibility zones. This combination of accuracy, granularity, and empirical validation positions this work as one of the most robust urban flood susceptibility assessments in the regional context.

4. Conclusions

A GIS-based AHP model is used in this study to assess and map the urban flood susceptibility for the city of Bhubaneswar using relevant geographical and spatial parameters. The outcomes of the analysis show the city's southern, south-eastern, and certain central and north-eastern portions to be the areas with higher susceptibility of urban flooding. This augmented risk stems from low elevation, dense urbanization, and high drainage density. Based on the central concepts of multi-criteria analysis, we determined that slope, LULC, drainage density, and rainfall are the major parameters for assessing flood susceptibility. Relative to other works of urban flood assessments in India and Southeast Asia regions, this model seems to indicate that the major factors such as rapid urban expansion, poor drainage, and infrequent rainfall are the dominating causes of flood susceptibility. This research adds to the literature on urban flood assessments in India and Southeast Asia. Unlike other urban flood models that depend on physical parameters, this approach underscores the value of coupling spatial and geo-physical variables in a more holistic approach. This study is unique in its kind, because it breaks the norm of urban flood risk evaluation models with its evidence-backed methodology. Generating a high-resolution flood susceptibility map enables us to assist urban planners and policy makers with critical information for emergency planning, infrastructure development, and sustainable land use strategies. For instance, in Bhubaneswar, these maps aid in designating flood-prone areas and determining the locations of flood shelters, emergency evacuation routes, and construction of safe housing zones. The results support the creation of anticipatory flood mitigation measures, thereby minimizing economic damage and risks to public safety. Besides, policymakers can use socio-demographic information (for example, population density, vulnerable communities, and critical infrastructure) and overlay with susceptibility maps to target high risk neighborhoods and prioritize interventions where social vulnerability intersects with physical exposure. However, along with its strength, this study has limitations. The exclusion of real-time hydrological data, socio-economic factors, and maticulate drainage system information may affect the precision of susceptibility assessments. An inclusion of integrated hydrodynamic models (for example, SWMM and HEC-RAS) that take into account the hydrological processes of surface runoff, infiltration, and drainage systems would enhance the analysis and the accuracy of predicting floods. Additionally, while AHP is a very popular analytical method, the reliance on the opinion of experts adds an element of subjectivity into the distribution of the weights. In future research, researchers should focus on the integration of real-time flood monitoring data, coupled with hydrodynamic modeling and machine learning, which would provide significant enhancements in techniques of predictive accuracy. Moreover, real-time early warning and alert systems tethered to the susceptibility maps on the framework of these major models would strengthen the overall preparedness for the impending disaster. Moreover, adding economic and social vulnerability factors is likely to improve the accuracy of flood risk assessments and the effectiveness of urban resilience planning. This the first study of its kind and offers a valuable methodological framework for urban flood risk assessment for areas undergoing rapid urban expansion. Its operationalization in Bhubaneswar illustrates the value of high-resolution susceptibility mapping to enhance municipal flood management and land-use policy formation, along with the development of the emergency response framework and associated policies. These results, along with a methodical approach, may be used for other urban areas that experience similar flooding difficulties, underscoring the role of geospatial data in risk reduction strategy planning.

Author contributions

Monashree Panigrahi: Conceptualization, Methodology, Data curation, Coding, Visualization, Writing original draft, Sudhakar Pal: Data Curation, Validation, Formal Analysis, Writing – Review & Editing. Arabinda Sharma*: Supervision, Resources, Review & Editing, Project Administration.

Use of AI tools declaration

The authors declare they have not used Artificial Intelligence (AI) tools in this article.

Acknowledgments

The authors declare that this research received no specific grant from any funding agency in the public, commercial, or not-for-profit sectors. However, the authors are thankful to all the anonymous reviewers whose comments help in improving the overall quality of the article.

Conflicts of interest

The authors hereby declare no conflict of interest.

References

1. Su M, Zheng Y, Hao Y, et al. (2018) The influence of landscape pattern on the risk of urban water-logging and flood disaster. *Ecol Indic* 92: 133–140. https://doi.org/10.1016/J.ECOLIND.2017.03.008
2. Roy S, Bose A, Chowdhury IR (2021) Flood risk assessment using geospatial data and multi-criteria decision approach: a study from historically active flood-prone region of Himalayan foothill, India. *Arab J Geosci* 14: 999. https://doi.org/10.1007/S12517-021-07324-8
3. Ghosh A (2017) Quantitative approach on erosion hazard, vulnerability and risk assessment: case study of Muriganga–Saptamukhi interfluve, Sundarban, India. *Nat Hazards* 87: 1709–1729. https://doi.org/10.1007/S11069-017-2844-0
4. Chowdary VM, Chandran RV, Neeti N, et al. (2008) Assessment of surface and sub-surface waterlogged areas in irrigation command areas of Bihar state using remote sensing and GIS. *Agric Water Manage* 95: 754–766. https://doi.org/10.1016/J.AGWAT.2008.02.009
5. Akilan A, Balaji S, Abdul Azeez K, et al. (2017) Source and causes of 2015 great pluvial flood of Chennai, Tamil Nadu and its surroundings. *J Geol Soc India* 90: 602–608. https://doi.org/10.1007/s12594-017-0758-9
6. Sahana M, Dutta S, Sajjad H (2019) Assessing land transformation and its relation with land surface temperature in Mumbai city, India using geospatial techniques. *Int J Urban Sci* 23: 205–225. https://doi.org/10.1080/12265934.2018.1488604
7. Jha CV, Bairagya H (2013) Flood and flood plains of West Bengal, India: A comparative analysis. *Rev Geoaraguaia* 3: 1–10.
8. Pathan AI, Agnihotri PG, Patel D, et al. (2021) Identifying the efficacy of tidal waves on flood assessment study—a case of coastal urban flooding. *Ara J Geosci* 14: 2132. https://doi.org/10.1007/S12517-021-08538-6
9. Kamat R (2019) Urban Flood Vulnerability Assessment of Bhopal, MP, India. *Int J Civil Eng Technol* 10: 2956–2977.

10. Ali SA, Khatun R, Ahmad A, et al. (2019) Application of GIS-based analytic hierarchy process and frequency ratio model to flood vulnerable mapping and risk area estimation at Sundarbans region, India. *Model Earth Syst Environ* 5: 1083–1102. https://doi.org/10.1007/S40808-019-00593-Z
11. Sarkar D, Mondal P (2020) Flood vulnerability mapping using frequency ratio (FR) model: a case study on Kulik river basin, Indo-Bangladesh Barind region. *Appl Water Sci* 10. https://doi.org/10.1007/s13201-019-1102-x
12. Khosravi K, Shahabi H, Pham BT, et al. (2019) A comparative assessment of flood susceptibility modelling using Multi-Criteria Decision-Making Analysis and Machine Learning Methods. *J Hydrol* 573: 311–323. https://doi.org/10.1016/J.JHYDROL.2019.03.073
13. Choubin B, Moradi E, Golshan M, et al. (2019) An ensemble prediction of flood susceptibility using multivariate discriminant analysis, classification and regression trees, and support vector machines. *Sci Total Environ* 651: 2087–2096. https://doi.org/10.1016/J.SCITOTENV.2018.10.064
14. Nazari R, Vasiliadis H, Maryam K, et al. (2022) Hydrodynamic Study of the Impact of Extreme Flooding Events on Wastewater Treatment Plants Considering Total Water Level. *Nat Hazards Rev* 23. https://doi.org/10.1061/(ASCE)NH.1527-6996.0000531
15. Siddiqui MZ, Everett JW, Vieux BE (1996) Landfill Siting Using Geographic Information Systems: A Demonstration. *J Environ Eng* 122: 515–523. https://doi.org/10.1061/(ASCE)0733-9372(1996)122:6(515)
16. Mishra P, Jena D, Thakur RR, et al. (2024) Peri-Urban Floodscapes: Identifying and Analyzing Flood Risk Areas in North Bhubaneswar in Eastern India. *Water* 16: 3019. https://doi.org/10.3390/W16213019
17. Islam T, Zeleke EB, Afroz M, et al. (2025) A Systematic Review of Urban Flood Susceptibility Mapping: Remote Sensing, Machine Learning, and Other Modeling Approaches. *Remote Sens* 17: 524. https://doi.org/10.3390/RS17030524
18. Khan ZA, Jhamnani B (2024) Development of flood susceptibility map using a GIS-based AHP approach: a novel case study on Idukki district, India. *J Spat Sci* 69: 409–442. https://doi.org/10.1080/14498596.2023.2236051
19. Sofi MS, Rautela KS, Muslim M,et al. (2024) From data to decisions: evaluating flood vulnerability in the Sindh watershed through Analytical Hierarchy Process. *FURP* 2: 1–16. https://doi.org/10.1007/S44243-024-00036-Z
20. Mondal KC, Saha S, Aitch P (2022) Flood hazards and risk prediction by using the Analytical Hierarchy Process on GIS platform: a case study in lower Ajay basin, India. *Disaster Adv* 16: 1–13.
21. Ahmed I, Das (Pan) N, Debnath J, et al. (2024) Flood hazard zonation using GIS-based multi-parametric Analytical Hierarchy Process. *GeoGeo* 3: 100250. https://doi.org/10.1016/J.GEOGEO.2023.100250
22. Bokhari BF, Tawabini B, Baalousha HM (2024) A fuzzy analytical hierarchy process -GIS approach to flood susceptibility mapping in NEOM, Saudi Arabia. *Front Water* 6: 1388003. https://doi.org/10.3389/frwa.2024.1388003
23. Arabameri A, Saha S, Chen W, et al. (2020) Flash flood susceptibility modelling using functional tree and hybrid ensemble techniques. *J Hydrol* 587. https://doi.org/10.1016/J.JHYDROL.2020.125007

24. Souissi D, Zouhri L, Hammami S, et al. (2020) GIS-based MCDM – AHP modeling for flood susceptibility mapping of arid areas, southeastern Tunisia. *Geocarto Int* 35: 991–1017. https://doi.org/10.1080/10106049.2019.1566405
25. Kanani-Sadat Y, Arabsheibani R, Karimipour F, et al. (2019) A new approach to flood susceptibility assessment in data-scarce and ungauged regions based on GIS-based hybrid multi criteria decision-making method. *J Hydrol* 572: 17–31. https://doi.org/10.1016/J.JHYDROL.2019.02.034
26. Tadono T, Ishida H, Oda F, et al. (2014) Precise Global DEM Generation by ALOS PRISM. *ISPRS Ann Photogramm Remote Sens Spatial Inf Sci* II–4: 71–76. https://doi.org/10.5194/ISPRSANNALS-II-4-71-2014
27. Zevenbergen LW, Thorne CR (1987) Quantitative analysis of land surface topography. *Earth Surf Process Landf* 12: 47–56. https://doi.org/10.1002/ESP.3290120107
28. Alshahrani S, Alshahrani HM, Tamizhselvi A, et al. (2024) Assessment of coastal vulnerability using AHP and machine learning techniques. *J South Am Earth Sci* 147. https://doi.org/10.1016/j.jsames.2024.105107
29. Bagyaraj M, Senapathi V, Chung SY, et al. (2023) A geospatial approach for assessing urban flood risk zones in Chennai, Tamil Nadu, India. *Environ Sci Pollut Res* 30: 100562–100575. https://doi.org/10.1007/s11356-023-29132-1
30. Sharma A (2010) Integrating terrain and vegetation indices for identifying potential soil erosion risk area. *Geo-Spat Inf Sci* 13: 201–209. https://doi.org/10.1007/S11806-010-0342-6
31. Panigrahi M, Sharma A (2025) Urban growth dynamics and its influence on land surface temperature in Bhubaneswar metropolitan city: a 1990–2021 analysis. *Discov Appl Sci* 7: 118. https://doi.org/10.1007/S42452-025-06535-Y
32. Panigrahi M, Sharma A (2024) Flood Vulnerability Mapping and Resilience in Urban Setting: A Review of Conceptual Frameworks and Assessment Methods. *Flood Risk Management. Springer Natural Hazards. Springer*, Singapore. 235–270. https://doi.org/10.1007/978-981-97-2688-2_11
33. Swain KC, Singha C, Nayak L (2020) Flood susceptibility mapping through the GIS-AHP technique using the cloud. *ISPRS Int J Geo-Inf* 9: 720. https://doi.org/10.3390/ijgi9120720
34. Sharma A, Tiwari KN (2014) A comparative appraisal of hydrological behavior of SRTM DEM at catchment level. *J Hydrol* 519: 1394–1404. https://doi.org/10.1016/J.JHYDROL.2014.08.062
35. Sutradhar C, Poddar D, Das J (2024) Optimization of conditioning factors for groundwater potential zonation using GIS-based single parameter and map removal sensitivity analysis in Alipurduar district of West Bengal, India. *Model Earth Syst Environ* 10: 1671–1694. https://doi.org/10.1007/s40808-023-01859-3
36. Abedi R, Costache R, Shafizadeh-Moghadam H, et al. (2022) Flash-flood susceptibility mapping based on XGBoost, random forest and boosted regression trees. *Geocarto Int* 37: 5479–5496. https://doi.org/10.1080/10106049.2021.1920636
37. Bui QT, Nguyen QH, Nguyen XL, et al. (2020) Verification of novel integrations of swarm intelligence algorithms into deep learning neural network for flood susceptibility mapping. *J Hydrol* 581: 124379. https://doi.org/10.1016/J.JHYDROL.2019.124379
38. Al-Juaidi AEM, Nassar AM, Al-Juaidi OEM (2018) Evaluation of flood susceptibility mapping using logistic regression and GIS conditioning factors. *Arab J Geosci* 11. https://doi.org/10.1007/S12517-018-4095-0

39. Dormann CF, Elith J, Bacher S, et al. (2013) Collinearity: A review of methods to deal with it and a simulation study evaluating their performance. *Ecography* 36: 27–46. https://doi.org/10.1111/j.1600-0587.2012.07348.x
40. Ramazi H, Amini A (2014) Fuzzy logic application in compiling multi geohazards macro-zone maps; case study: Rahdar, 1:25,000 Quadrangle, Khuzestan, Iran. *Arab J Geosci* 7: 3243–3249. https://doi.org/10.1007/S12517-013-0943-0
41. Shrestha N (2020) Detecting Multicollinearity in Regression Analysis. *Am J Appl Math Stat* 8: 39–42. https://doi.org/10.12691/AJAMS-8-2-1
42. Saaty TL (1977) A scaling method for priorities in hierarchical structures. *J Math Psychol* 15: 234–281. https://doi.org/10.1016/0022-2496(77)90033-5
43. Mann R, Gupta A (2023) Mapping flood vulnerability using an analytical hierarchy process (AHP) in the Metropolis of Mumbai. *Environ Monit Assess* 195. https://doi.org/10.1007/s10661-023-12141-5
44. Bansal N, Mukherjee M, Gairola A (2023) GIS-based multi-criteria decision analysis for mapping flood-prone areas in Dehradun city, India. *Arab J Geosci* 16. https://doi.org/10.1007/s12517-023-11605-9
45. Khumaeroh DNF, Sari DN (2024) Application of Analytical Hierarchy Process (AHP) and Geographic Information System (GIS) in flood hazard analysis in the Rawa Pening Sub-Watershed, Indonesia. *IOP Conf Ser Earth Environ Sci*, 1314. https://doi.org/10.1088/1755-1315/1314/1/012114
46. Triantaphyllou E, Mann SH (1995) Using the Analytic Hierarchy Process for Decision Making in Engineering Applications: Some Challenges. *J Ind Eng Appl Pract* 2: 35–44.
47. Saaty TL (1990) How to make a decision: The analytic hierarchy process. *Eur J Oper Res* 48: 9–26. https://doi.org/10.1016/0377-2217(90)90057-I
48. Ouma YO, Tateishi R (2014) Urban flood vulnerability and risk mapping using integrated multi-parametric AHP and GIS: Methodological overview and case study assessment. *Water* 6: 1515–1545. https://doi.org/10.3390/w6061515
49. Lv H, Guan X, Meng Y (2020) Comprehensive evaluation of urban flood-bearing risks based on combined compound fuzzy matter-element and entropy weight model. *Nat Hazards* 103: 1823–1841. https://doi.org/10.1007/S11069-020-04056-Y
50. Manfreda S, Nardi F, Samela C, et al. (2014) Investigation on the use of geomorphic approaches for the delineation of flood prone areas. *J Hydrol* 517: 863–876. https://doi.org/10.1016/J.JHYDROL.2014.06.009
51. Chini M, Pelich R, Li Y, et al. (2021) SAR-based Flood Mapping, Where We Are and Future Challenges. *International Geoscience and Remote Sensing Symposium IGARSS*, IEEE, 884–886. https://doi.org/10.1109/IGARSS47720.2021.9554975
52. Dhanabalan SP, Rahaman SA, Jegankumar R (2019) Flood monitoring using Sentinel-1 sar data: A case study based on an event of 2018 and 2019 southern part of Kerala. *Int Arch Photogramm Remote Sens Spatial Inf Sci*, 37–41. https://doi.org/10.5194/isprs-archives-XLIV-M-3-2021-37-2021
53. Shahabi H, Shirzadi A, Ghaderi K, et al. (2020) Flood Detection and Susceptibility Mapping Using Sentinel-1 Remote Sensing Data and a Machine Learning Approach: Hybrid Intelligence of Bagging Ensemble Based on K-Nearest Neighbor Classifier. *Remote Sens* 12: 266. https://doi.org/10.3390/RS12020266

54. Garg S, Dasgupta A, Motagh M, et al. (2024) Unlocking the full potential of Sentinel-1 for flood detection in arid regions. *Remote Sens Environ* 315: 114417. https://doi.org/10.1016/J.RSE.2024.114417
55. Tanim AH, McRae CB, Tavakol-davani H, et al. (2022) Flood Detection in Urban Areas Using Satellite Imagery and Machine Learning. *Water* 14: 1140. https://doi.org/10.3390/W14071140
56. Yu J, Wu M, Li C, et al. (2020) A SAR image segmentation method based on otsu and level set. *2020 IEEE 9th Joint International Information Technology and Artificial Intelligence Conference (ITAIC)*, IEEE, 9: 2189–2193. https://doi.org/10.1109/ITAIC49862.2020.9339053
57. Amitrano D, Di Martino G, Di Simone A, et al. (2024) Flood Detection with SAR: A Review of Techniques and Datasets. *Remote Sens* 16: 656. https://doi.org/10.3390/RS16040656
58. Murray L, Nguyen H, Lee YF, et al. (2012) Variance Inflation Factors in Regression Models With Dummy Variables. *Conference on Applied Statistics in Agriculture*. https://doi.org/10.4148/2475-7772.1034
59. Kim JH (2019) Multicollinearity and misleading statistical results. *Korean J Anesthesiol* 72: 558–569. https://doi.org/10.4097/KJA.19087
60. Neter J, Kutner MH, Nachtsheim CJ (2005) *Applied linear statistical models*. McGraw-Hill Irwin.
61. Gao BC (1996) NDWI—A normalized difference water index for remote sensing of vegetation liquid water from space. *Remote Sens Environ* 58: 257–266. https://doi.org/10.1016/S0034-4257(96)00067-3
62. Xu H (2006) Modification of normalised difference water index (NDWI) to enhance open water features in remotely sensed imagery. *Int J Remote Sens* 27: 3025–3033. https://doi.org/10.1080/01431160600589179
63. Mohammadi A, Kamran KV, Karimzadeh S, et al. (2020) Flood Detection and Susceptibility Mapping Using Sentinel-1 Time Series, Alternating Decision Trees, and Bag-ADTree Models. *Complexity* 2020: 4271376. https://doi.org/10.1155/2020/4271376
64. Xu H (2006) Modification of normalised difference water index (NDWI) to enhance open water features in remotely sensed imagery. *Int J Remote Sens* 27: 3025–3033. https://doi.org/10.1080/01431160600589179
65. Li Z, Zhang X, Ma Y, et al. (2019) A multi-criteria decision making method for urban flood resilience evaluation with hybrid uncertainties. *Int J Disaster Risk Reduct* 36. https://doi.org/10.1016/j.ijdrr.2019.101140
66. Lee BJ, Kim S (2019) Gridded Flash Flood Risk Index Coupling Statistical Approaches and TOPLATS Land Surface Model for Mountainous Areas. *Water* 11: 504. https://doi.org/10.3390/W11030504
67. Fernández DS, Lutz MA (2010) Urban flood hazard zoning in Tucumán Province, Argentina, using GIS and multicriteria decision analysis. *Eng Geol* 111: 90–98. https://doi.org/10.1016/J.ENGGEO.2009.12.006
68. Dhiman R, Kalbar P, Inamdar AB (2018) GIS coupled multiple criteria decision making approach for classifying urban coastal areas in India. *Habitat Int* 71: 125–134. https://doi.org/10.1016/J.HABITATINT.2017.12.002
69. Hasan MM, Mondol Nilay MS, Jibon NH, et al. (2023) LULC changes to riverine flooding: A case study on the Jamuna River, Bangladesh using the multilayer perceptron model. *Results Eng* 18: 101079. https://doi.org/10.1016/J.RINENG.2023.101079
70. Bay C, Glynn RJ, Seddon JM, et al. (2023) Evaluation of Risk Prediction with Hierarchical Data: Dependency Adjusted Confidence Intervals for the AUC. *Stats* 6: 526–538. https://doi.org/10.3390/STATS6020034

71. Mandal KK, Dharanirajan K, Meena ML, et al. (2023) Application of geospatial tools in the assessment of Flood hazard impact on social vulnerability of Malda district, West Bengal, India. *Nat Hazards Res* 4: 470–485. https://doi.org/10.1016/J.NHRES.2023.11.008
72. Wang Z, Ma C, Zhang Y, et al. (2023) Assessment of urban flooding vulnerability based on AHP-PSR model: a case study in Jining City, China. *Geocarto Int* 38. https://doi.org/10.1080/10106049.2023.2252777
73. Das S (2020) Flood susceptibility mapping of the Western Ghat coastal belt using multi-source geospatial data and analytical hierarchy process (AHP). *Remote Sens Appl* 20: 100379. https://doi.org/10.1016/J.RSASE.2020.100379
74. Khan ZA. Jhamnani B (2024) Development of flood susceptibility map using a GIS-based AHP approach: a novel case study on Idukki district, India. *J Spat Sci* 69: 409–442. https://doi.org/10.1080/14498596.2023.2236051
75. Das S, Gupta A (2021) Multi-criteria decision based geospatial mapping of flood susceptibility and temporal hydro-geomorphic changes in the Subarnarekha basin, India. *Geosci Front* 12: 101206. https://doi.org/10.1016/j.gsf.2021.101206
76. Murali KV, Srinivasan K (2025) GIS and AHP Based Flood Susceptibility Mapping: A Case Study of Chalakudy River Basin, Kerala, India. *Int J Environ Clim Change* 15: 18–34. https://doi.org/10.9734/IJECC/2025/V15I94992

AIMS Press